International Journal of Nanoelectronics and Materials
Volume 15 (Special Issue) December 2022 [389-398]

Electrical Simulation on Silicon Nanowire Field-effect Transistor Biosensor at Different Substrate-gate Voltage Bias Conditions for Charge Detection

X.Y. Teoh[2], M.F.M. Fathil[1], Y.M.Tan[2], N. Sabani[2], M.N.M. Nuzaihan[1], M.K. Md Arshad[1, 2], A.R. Ruslinda[1], N.H.A. Halim[1], R.M. Ayub[1], U. Hashim[1], and M.M. Ibrahim[3]

[1]Institute of Nano Electronic Engineering, Universiti Malaysia Perlis, 01000 Kangar, Perlis, Malaysia
[2]Faculty of Electronic Engineering & Technology, Universiti Malaysia Perlis, 02600 Arau, Perlis, Malaysia
[3]Centre for Telecommunication Research and Innovation, Faculty of Electronic and Computer Engineering, Universiti Teknikal Malaysia Melaka, Malaysia

ABSTRACT

In this work, the impact of different substrate-gate voltage bias conditions (below and above the device threshold voltage) on current-voltage characteristics and sensitivity of a silicon nanowire field-effect transistor (SiNW-FET) biosensor was investigated. A 3-dimensional device structure with n-type SiNW channel and a substrate gate electrode was designed and electrically simulated In the Silvaco ATLAS. Next, the SiNW channel was covered with a range of interface charge density to mimic the charged target biomolecule captured by the device. The outcome was translated into a drain current versus interface charge semi-log graph and the device sensitivity was calculated using the linear regression curve's slope of the plotted data. The device's electrical characteristic shown higher generation of output drain current values with the increase of negative substrate-gate voltage bias due to the hole carriers' accumulation that forms a conduction channel in the SiNW. Application of higher negative interface charge density increased the change in drain current, with the device biased with higher substrate-gate voltage shows more significant change in drain current. The device sensitivity increased when biased with higher substrate-gate voltage with highest sensitivity is 75.12 nA/dec at substrate-gate voltage bias of –1.00 V.

Keywords: Biosensor, field effect-transistor, silicon nanowire, silicon-on-insulator, substrate-gate voltage bias

1. INTRODUCTION

Biosensor, an analytical device which integrates the bioreceptor and transducer for converting biological response into measurable signal [1], have been around since its introduction in 1962 by Clark and Lyons [2] for variety of applications including in monitoring of health [3,4], environment [5], as well as quality of food [6,7] and water [8]. In the recent years, silicon nanowire-based field-effect transistor (SiNW-FET) has attracted much attention among diverse type of biosensors for medical related application due to it significant advantages such as high sensitivity and selectivity with the rapid detection capability of biomolecules as big as proteins and enzymes to as small as deoxyribonucleic acid (DNA), ribonucleic acid (RNA) and viruses. It also enables reproducibility and miniaturization due to its compatibility with top-down manufacturing process and complementary metal-oxide-semiconductor (CMOS) technology. Technology computer-aided design (TCAD) software, which is commonly used in the semiconductor devices design simulation can also be simply adapted for the design of the SiNW-FET biosensor [9,10].

* mohamadfaris@unimap.edu.my

The SiNW-FET is designed as a three-electrode system with SiNW channel connected to the source and drain electrodes, while the gate electrode modulates the channel's conductance [11]. SiNW can be fabricated using either top-down (using chemical vapor deposition) or bottom-up technique (using e-beam lithography). Then, the surface of the SiNW channel is immobilized with strong affinity biological receptors such as monoclonal antibodies or single-strand DNA (ssDNA) probes by chemical modification for distinguishing the target biomolecules with high specificity [12]. The binding event between charged biomolecule with their respective bioreceptor somehow comparable to supplying voltage to the gate electrode in a conventional metal-oxide-semiconductor FET (MOSFET), that give rise to a charge variation at the SiNW surface [13]. This event contributes to the carriers' depletion or accumulation near the SiNW channel's surface area, thus causes the conductance change. When positively or negatively charged biomolecules bind onto its surface, carriers' depletion or accumulation may occur in the *p*-type SiNW channel, leading to decrease or increase of output drain current (I_D) of the biosensor, respectively. On the other hand, opposite behaviour can be observed for *n*-type SiNW channel [11]. High sensitivity detection of the binding even can be achieved with the SiNW channel is comparable to the size of the target biomolecules [14].

The deployment of wafer made of silicon-on-insulator (SOI), a semiconductor structure comprising of a single crystalline silicon (Si) layer split from the bulk Si substrate by a thin layer of insulator [15], has been reported for fabrication of the SiNW-FET biosensor [4]. In a top-down fabrication approach of a device, the thin insulator also known as buried oxide (BOx) layer is convenient to be used as an etch-stop layer for patterning the nanostructure at the top Si layer. SOI also provides a specific phenomenon called dual-gate configuration which can be exploited to enhance the device performance for sensing application [16], which comprises of charged biomolecules detection at the front gate of the channel surface and amplified shift when reading the output signal with the substrate-gate [17–20].

The SOI-based SiNW-FET biosensor requires V_{SG} for the device operation and to become more responsive towards charge target biomolecule detection. With the proper V_{SG} bias, the signal can be amplified internally [21]. Hence, in this work, the effect of V_{SG} bias on the electrical behaviour of a SiNW-FET biosensor and its charge detection performance was investigated. This work was implemented with the aid of Silvaco ATLAS device simulator software for structure design and electrical simulations of the device with several V_{SG} bias condition, which include below and above the threshold voltage (V_T), where the change in I_D was observed and analysed. Further simulations and analysis were performed with the application of interface charges on the SiNW channel surface towards the performance of the device in terms of sensitivity for charged biomolecules detection. The results at different V_{SG} bias were compared to observe the device performance improvement in biosensing application.

2. METHODS

2.1 Structural Design Specifications

Silvaco ATLAS device simulation software was used in conjunction with the DeckBuild run-time environment to execute a list of commands in an American Standard Code for Information Interchange (ASCII) text file known as input file. Prior to the design of the SiNW-FET biosensor structure, initial statement definition of mesh was specified in the input file. The mesh covers the domain of physical simulation represented by grid made of horizontal and vertical lines that have spacing between them. Next, every part of the biosensor including substate, buried oxide, source, drain, SiNW channel and biomolecules interaction layer were assigned within previously specified mesh by defining the region statements. To enable electrical connectivity to the device, electrode statements was defined to assign aluminium electrodes at the location above the source, drain, and substrate regions. The device structure was finalised with the definition of specific doping concentration the at Si region including source, SiNW channel, drain and substrate regions using the doping statement for electrical conductivity. The parameters of the regions and electrodes with their respective materials used in the SiNW-FET biosensor construction are listed in Table 1 with its schematic diagram as in Figure 1.

2.2 Electrical Simulation Specifications

The electrical behaviour of SiNW-FET biosensor was obtained by simulation of the device structure. Necessary statements related to contact, interface charges, physical models, numerical methods, log, solve and save are included in the input files. The contact statement was set as neutral to indicate ohmic behaviour for the aluminium (Al) electrodes on the heavily doped *p*-type drain, source, and substrate-gate regions. Then, the interface statement was assigned to the device for applying interface charges density (Q_F) at the biomolecule interaction site made of silicon dioxide (SiO_2) in unit of electronic charges per square centimetre (*e*.cm^{-2}). The applied Q_F in the device simulation were in the range of -5×10^{10} *e*.cm^{-2} to -9×10^{10} *e*.cm^{-2}, to signify the charge density from target biomolecules bounded with the bioreceptor at site of biomolecule interaction over the channel of SiNW [17–20]. The physical models which include Fermi- Dirac carrier statistics (FERMIDIRAC) and Bandgap Narrowing (BGN) for the carrier statistics model, Lombardi transverse field dependent mobility (CVT) for the mobility model, Shockley-Read-Hall (SRH) for the recombination model, and Selberherr's Model (IMPACT SELB) for impact ionization were then selected and enabled for the device simulation. The physical models of SRH, FERMIDIRAC and CVT are recommended since the device structure is related to a non-planar MOSFET device, with addition of BGN model for simulation of device structure based on SOI wafer with the heavily doped drain and source regions (more than 10^{18} atoms/cm^3). Next, the bi-conjugate gradient stability (BICGST) was enabled as the linear iterative method to allow most efficient 3D simulation due to reduced memory usage and solution times. The physical models and numerical method were chosen and enabled based on the recommendation from the ATLAS user manual and simulation examples for SOI MOSFET devices provided in the simulation software. The electrical biasing on the device was performed by using solve statement while the solution was tabulated and save using log statement. The initial simulation was performed for producing the transfer characteristic to determine the V_T of the device with drain voltage (V_D) bias of −10 mV and substrate-gate voltage (V_{SG}) sweep from 0 V to −1.00 V. Based on the finding, several V_{SG} (below and above V_T) was chosen and biased during V_D sweep from 0 V to −1.00 V to observe the impact on the output I_D of the device.

Table 1 Design parameters of the SiNW-FET biosensor

Regions	Materials	Dopant Type/ Concentration (atoms/cm^3)	Length (μm)	Width (nm)	Thickness (nm)
Substrate	Si	*p*-type / 1×10^{15}	10.0	100	500
BOx	SiO_2	-	7.0	100	100
Source / Drain	Si	*p*-type / 5×10^{19}	0.9	100	30
SiNW	Si	*n*-type / 1×10^{17}	5.2	30	30
Biomolecule interaction site (left- / right-side)	SiO_2	-	5.0	11	30
Biomolecule interaction site (top-side)	SiO_2	-	5.0	52	11
Electrodes	Al	-	0.9	100	60

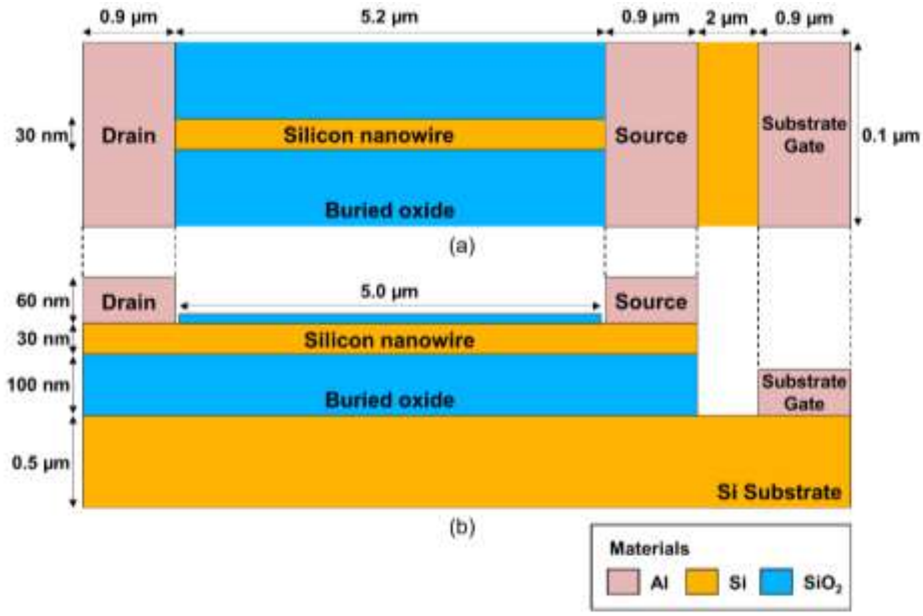

Figure 1. The (a) top- and (b) side-views of the SiNW-FET biosensor Schematic diagram.

2.3 Sensitivity Calculation and Analysis

The I_D values at V_D of −1.00 V from the produced output characteristics when the device applied with various Q_F during all V_{SG} biases were extracted. These data were used to plot the I_D versus Q_F semi-log graph, and a linear regression curve can be developed from the plotted data. The sensitivity of the SiNW-FET was determined by referring to the slope of the linear regression curve based on Equation (1) [22]:

$$\text{Sensitivity} = \frac{\Delta I_D}{\Delta Q_F} \quad (1)$$

where ΔI_D is change in I_D and ΔQ_F is change in Q_F. The calculation for ΔI_D is straight-forward as in Equation (2) [22]:

$$\Delta I_D = |I_{D2} - I_{D2}| \quad (2)$$

where I_{D1} and I_{D2} are I_D at two different points on the linear regression curve with the ΔI_D unit is in ampere (A). However, since logarithmic scale was used for the *x*-axis of the semi-log plot, the ΔQ_F was calculated as in Equation (3) [23]:

$$\Delta Q_F = \log_{10} Q_{F2} - \log_{10} Q_{F1} = \log_{10}\left(\frac{Q_{F2}}{Q_{F1}}\right) \quad (3)$$

where Q_{F1} and Q_{F2} are the Q_F at the two previous points on the linear regression curve, which are I_{D1} and I_{D2}, respectively. Notice that, the division operation of Q_{F1} and Q_{F2} in Equation (4) causes their units to cancel each other. The $\log_{10}$ in the equation allows ΔQ_F unit to be denoted in decade (dec). Therefore, the unit for *S* in this study is represented in terms of ampere per decade (A/dec). The sensitivity of the device was compared based on the different bias of V_{SG}.

3. RESULTS AND DISCUSSION

3.1 Device Structural Design

Figure 2 shows the 3D structure of the SiNW-FET in TonyPlot of Silvaco Atlas device simulation software. The structure was designed with consideration of using SOI wafer in its fabrication process. The base Si region acts as the substrate of the device, followed by a 100-nm thick SiO_2, also BOx layer as the substrate-gate dielectric material, and finally another Si layer cover on top, which serve as the device layer with thickness of 30 nm. The device layer consists of drain and source regions with width of 100 nm connected by a 5.2-µm long SiNW channel with the width of 30 nm which is the transducer of the device for sensing the charges exhibit by target biomolecules. The SiNW channel's surface was blanketed by another 5.0-nm thick SiO_2 layer, which serve as the biomolecule interaction site to allows covalent binding of many different biomolecules as bioreceptors (e.g., DNAs, aptamers, antibodies, enzymes, and whole cells) for identifying specific target biomolecule with proper surface modification procedures [24,25]. The electrodes for the source, drain, and substrate-gate were made of aluminium with thickness of 60 nm for electrical connectivity. High dopant concentration (5×10^{19} atom/cm^3) for the source and drain regions using *p*-type dopant to allow ohmic contact between the Si and Al electrodes [26,27]. To form the *p*-channel enhancement-mode operation of FET, the SiNW channel was doped with *n*-type dopant at 1×10^{17} atom/cm^3 [28].

3.2 Simulated Device Electrical Characteristics

When the device is electrically simulaed in Silvaco ATLAS, similar electrical characteristic of a *p*-channel enhancement mode MOSFET [28] was exhibited by the SiNW-FET biosensor as shown in Figure 3. From the transfer characteristic in Figure 3(a), there was no output I_D during the cut-off state when the device was biased with V_{SG} that is lower than the V_T ($|V_{SG}| < |V_T|$) since the *p*-type drain and source regions are set apart by the *n*-type SiNW channel, resembling two back-to-back diodes. Only after V_{SG} was equal or greater than the V_T ($|V_{SG}| \geq |V_T|$), the holes inversion layer was created that allows holes flow from the source to drain when a small V_D of −10 mV was applied to the device. Induction by electric field of hole inversion layer in the oxide-semiconductor interface of *n*-type SiNW channel requires only a negative V_{SG} bias. Therefore, I_D can flow into the source and out of the drain regions and the current is greater with larger V_{SG} [28].

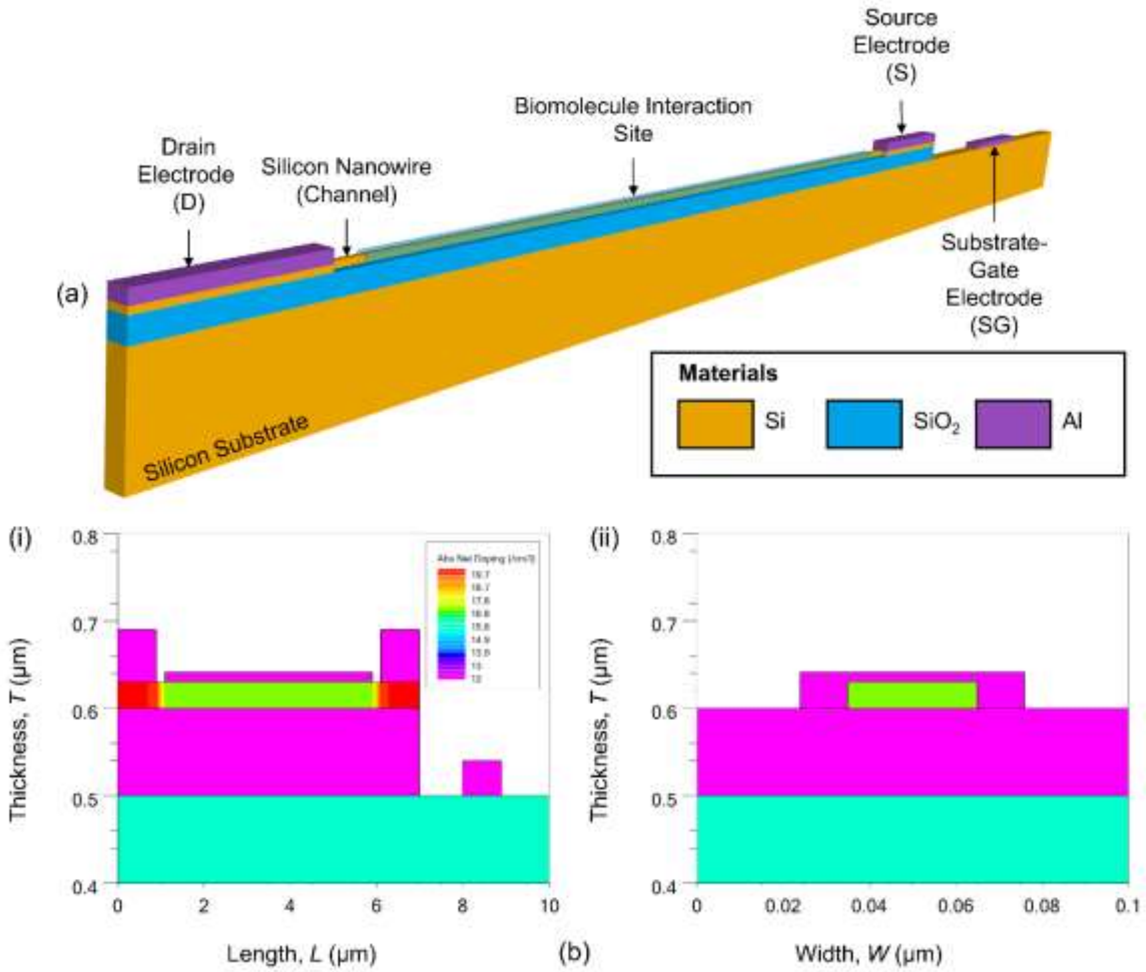

Figure 2. SiNW-FET Biosensor device structure in (a) 3-dimensional perspective view and (b) 2D cross-sectional views showing doping concentration (i) along and (ii) across the device.

Using linear extrapolation (LE) method in the linear region [29], the V_T of the device was located at –0.654 V. The extraction of V_T is crucial for determining and selecting appropriate values of V_{SG} to study its impact on the device sensitivity as biosensor for charge detection. Therefore, several different V_{SG} bias conditions were chosen in this work, which are below (V_{SG} of –0.50 V) and above V_T (V_{SG} of –0.75 V and –1.00 V) with the simulated output characteristic of the device can be seen in Figure 3(b). As V_{SG} of –0.50 V was biased to the device along with the increasing applied V_D to –1.00 V, I_D remains near to 0 A due to insufficient V_{SG} to turn on the device. However, as V_{SG} bias was increased to –0.75 V, the I_D begun to increase to –0.492 nA at V_D of –1.00 V. Finally, at V_{SG} of –1.00 V, the device's I_D shows the highest measured value of I_D at –4.407 nA, which is almost 9 times greater than the previous V_{SG} bias. The relationship between I_D in the saturation region ($I_{D(sat)}$) and V_{SG} can be expressed by Equation (4) [28]:

$$I_{D(sat)} = \frac{W}{2L}\mu_p C_{ox}(V_{SG} - V_T)^2 \quad (4)$$

where W, L, and C_{ox} are the channel width, channel length, and buried oxide capacitance per unit area, respectively, while the μ_p is the hole mobility in the hole inversion layer. Thus, greater V_{SG} bias to the device affect the device electrical performance by boosting the output I_D flow along the channel of the SiNW between drain and source region.

The device capability for charge detection can be observed as in Figure 4 where the effect of Q_F on I_D at previously chosen V_{SG} bias of −0.50 V, −0.75 V and −1.00 V to the substrate-gate electrode of the device. Several negatively Q_F values, which are -5×10^{10} e·cm^{-2}, -6×10^{10} e·cm^{-2}, -7×10^{10} e·cm^{-2}, -8×10^{10} e·cm^{-2} and -9×10^{10} e·cm^{-2} were placed at the location of the occurrence biomolecule interaction on the SiNW channel. The device V_D was swept from 0 V to −1.00 V with step voltage of 0.05 V. For all tested V_{SG} bias, with the increase of negatively Q_F applied on the SiNW surface, the output I_D was increased. This event occurs because as more negative QF was applied on the SiNW channel, it attracted more holes (the minority carrier inside the *n*-type SiNW) to the hole inversion layer along the SiNW channel and allowed more current flow from source to drain regions. Although the same trend can be seen for all V_{SG} bias applied on the device, the I_D value is greater in the device with V_{SG} bias higher than the V_T especially when V_{SG} bias was −1.00 V, exhibiting more significant difference in I_D value for each application of Q_F value. The comparison of I_D for every application of Q_F values on the device at each V_{SG} bias is demonstrated as in Figure 4(d).

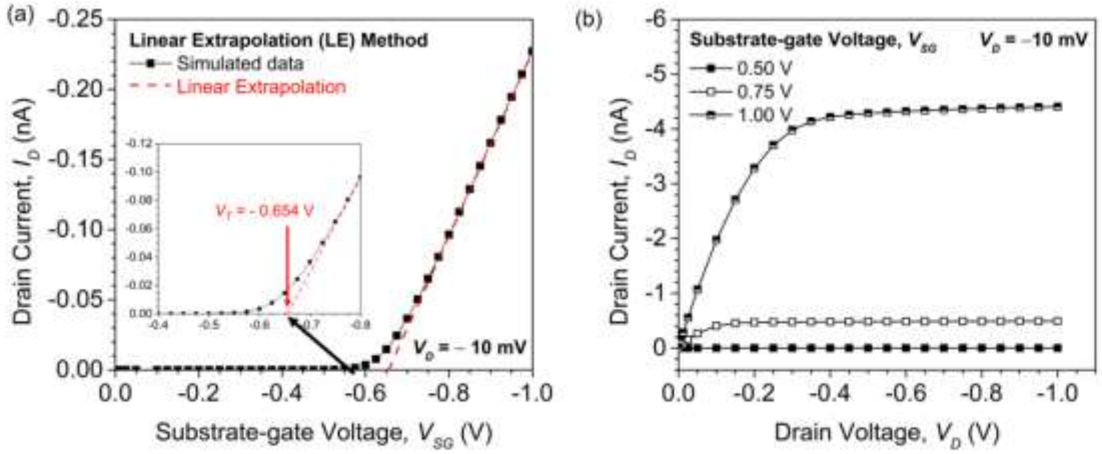

Figure 3. Electrical characteristics of the SiNW-FET Biosensor. (a) Transfer characteristic of the device biased at −10 mV of V_D with V_{SG} sweeps from 0 V to −1.00 V for V_T extraction using linear extrapolation (LE) method. (b) Output characteristics of the device with V_D sweep from 0 V to −1.00 V at V_{SG} bias of −0.50 V, −0.75 V, and -1.00 V.

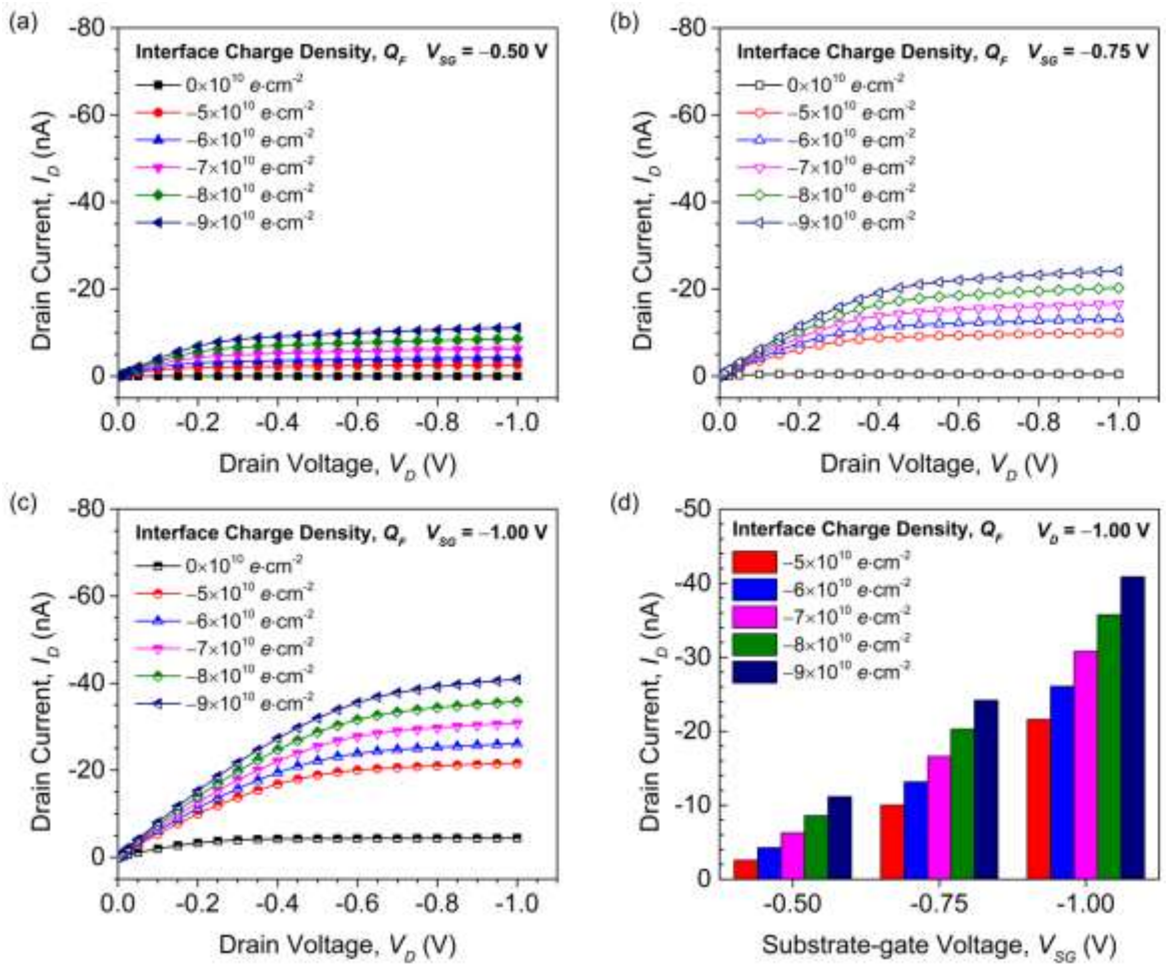

Figure 4. I-V characteristics of the SiNW-FET biosensor at V_{SG} bias of (a) −0.50 V, (b) −0.75 V and (c) −1.00 V with (d) comparison of the device output I_D at V_D of −1.00 V during charge detection.

3.3 Device Sensitivity Analysis

Based on the calculation using Equation (1), the result shows higher V_{SG} bias allow increase in device sensitivity, significantly as in Figure 5. SiNW-FET biosensor biased with the V_{SG} of −1.00 V produced the best sensitivity at 75.12 nA/dec when compared with the same device at lower V_{SG} bias of −0.75 V and −0.50 V with sensitivity of 55.22 nA/dec and 33.37 nA/dec, respectively. The increase in sensitivity is more than double when the same device was biased with V_{SG} from −0.50 V to −1.00 V. This result demonstrates that the device with V_{SG} of −1.00 V deliver considerable change in I_D when different charge density cover on the surface of the SiNW. Curve fitting of the linear regression for device applied with V_{SG} of −1.00 V shows a good R-squared, R^2 value which is 0.983 compared to device applied with −0.50 V and −0.75 V, only R^2 values of 0.963 and 0.978, respectively. The R^2 value indicates a goodness-of-fit measure for the linear regression model.

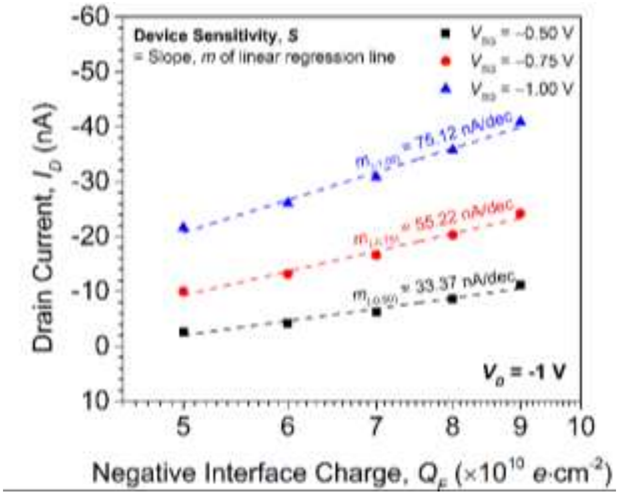

Figure 5. Sensitivity determination of the SiNW-FET biosensor biased at V_{SG} of –0.50 V, –0.75 V, and –1.00 V from the linear regression line slope, *m* of I_D versus Q_F semi-log plot.

4. CONCLUSION

The SiNW-FET biosensor was constructed and simulated in the Silvaco ATLAS to understand V_{SG} bias effect on its electrical behaviour and performance for charge detection. The device structure design based on the *p*-channel enhancement mode MOSFET demonstrated increased in output I_D with the increased of V_{SG} from below (V_{SG} of –0.50 V) to above (V_{SG} of –0.75 V and –1.00 V) the V_T. No current output was expected and observed at V_{SG} bias below the V_T as the device in cut-off state. The increase in minority carrier holes in holes inversion layer formed along the oxide-SiNW interface had caused the rise of current flow owing to the increase in generated electric field magnitude with the increase of negative V_{SG} above the V_T. The device demonstrated charge detection capability, even in the condition of V_{SG} below V_T, credits to the utilization of SiNW channel as transducer, which is sensitive to the influence of the Q_F applied to the location where biomolecule interact on its surface. With the increase of negative Q_F representing negatively charged biomolecule, the device exhibited significant increase in output current, especially when biased with V_{SG} as high as –1.00 V. The sensitivity analysis by using slope of linear regression curve in the I_D versus Q_F semi-log plot also revealed higher sensitivity can be obtained at 75.12 nA/dec when the SiNW-FET biosensor was biased with –1.00 V compared to the lower V_{SG} bias. Therefore, the V_{SG} bias does play a role in improving the device performance for detection of specific target biomolecule at specific concentration. However, it is not recommended to bias the device with very high V_{SG} since it may cause saturation in flow of current along the channel of SiNW, which in consequence making the device insensitive for charge detection on its surface, as well as high power consumption in the device operation.

ACKNOWLEDGEMENTS

The authors would like to acknowledge the support from the Fundamental Research Grant Scheme (FRGS) under a grant number of FRGS/1/2018/STG07/UNIMAP/02/7 from the Ministry of Higher Education, Malaysia. The authors also would like to acknowledge all the team members in Institute of Nano Electronic Engineering (INEE) and Faculty of Electronic & Engineering Technology (FKTEN), Universiti Malaysia Perlis (UniMAP) for their guidance and help related to this study.

REFERENCES

[1] Naresh, V. and Lee, N., Sensors 21, 1109 (2021).
[2] Clark, L.C. and Lyons, C., Ann. N.Y. Acad. Sci. 102, 29 (2006).
[3] Ahmad, R., Mahmoudi, T., Ahn, M.-S., and Hahn, Y.-B., Biosens. Bioelectron. 100, 312 (2018).
[4] Syu, Y.-C., Hsu, W.-E., and Lin, C.-T., ECS J. Solid State Sci. Technol. 7, Q3196 (2018).
[5] Elli, G., Ciocca, M., Lugli, P., and Petti, L., in 2021 IEEE Int. Work. Metrol. Agric. For. (IEEE, 2021), pp. 102–107.
[6] Hideshima, S., Saito, M., Fujita, K., Harada, Y., Tsuna, M., Sekiguchi, S., Kuroiwa, S., Nakanishi, T., and Osaka, T., Sensors Actuators B Chem. 254, 1011 (2018).
[7] Wang, Y., Bi, Y., Wang, R., Wang, L., Qu, H., and Zheng, L., J. Agric. Food Chem. 69, 1398 (2021).
[8] Mills, G. and Fones, G., Sens. Rev. 32, 17 (2012).
[9] Ajay, Narang, R., Saxena, M., and Gupta, M., Microsyst. Technol. 23, 3149 (2017).
[10] Nozaki, D., Kunstmann, J., Zörgiebel, F., Pregl, S., Baraban, L., Weber, W. M., Mikolajick, T., and Cuniberti, G., Nano Res. 7, 380 (2014).
[11] Gao, A., Chen, S., Wang, Y., and Li, T., Sensors Mater. 30, 1619 (2018).
[12] Chen, K.-I., Li, B.-R., and Chen, Y.-T., Nano Today 6, 131 (2011).
[13] Zhang, A., Zheng, G., and Lieber, C.M., in (2016), pp. 255–275.
[14] Gao, X.P.A., Zheng, G., and Lieber, C.M., Nano Lett. 10, 547 (2010).
[15] Mäkinen, J. and Suni, T., in Handb. Silicon Based MEMS Mater. Technol. (Elsevier, 2020), pp. 215–246.
[16] Benea, L.P., Out-of-Equilibrium Body Potential Measurements on SOI Substrates : Implementation and Applications, IMEP-LaHC, Université Grenoble Alpes, 2019.
[17] Accastelli, E., Cappi, G., Buckley, J., Ernst, T., and Guiducci, C., in 2013 13th IEEE Int. Conf. Nanotechnol. (IEEE-NANO 2013) (IEEE, 2013), pp. 517–520.
[18] Ayele, G.T., Monfray, S., Ecoffey, S., Boeuf, F., Bon, R., Cloarec, J.-P., Drouin, D., and Souifi, A., in 2018 IEEE Symp. VLSI Technol. (IEEE, 2018), pp. 97–98.
[19] Huang, Y.-J., Lin, C.-C., Huang, J.-C., Hsieh, C.-H., Wen, C.-H., Chen, T.-T., Jeng, L.-S., Yang, C.-K., Yang, J.-H., Tsui, F., Liu, Y.-S., Liu, S., and Chen, M., in 2015 IEEE Int. Electron Devices Meet. (IEEE, 2015), pp. 29.2.1-29.2.4.
[20] Jang, H.-J. and Cho, W.-J., Sci. Rep. 4, 5284 (2015).
[21] Naumova, O.V. and Zaytseva, E.G., Sensors 22, 2460 (2022).
[22] Nuzaihan, M.M.N., Hashim, U., Md Arshad, M.K., Kasjoo, S.R., Rahman, S.F.A., Ruslinda, A.R., Fathil, M.F.M., Adzhri, R., and Shahimin, M.M., Biosens. Bioelectron. 83, 106 (2016).
[23] Cornish-Bowden, A., Basic Mathematics for Biochemists (Springer Netherlands, Dordrecht, 1981).
[24] Mu, L., Chang, Y., Sawtelle, S.D., Wipf, M., Duan, X., and Reed, M.A., IEEE Access 3, 287 (2015).
[25] Sciuto, E.L., Bongiorno, C., Scandurra, A., Petralia, S., Cosentino, T., Conoci, S., Sinatra, F., and Libertino, S., Chemosensors 6, 59 (2018).
[26] Bandaru, P.R., Faraby, H., and DiBattista, M., J. Nanosci. Nanotechnol. 15, 9315 (2015).
[27] Paul, F., Nama Manjunatha, K., Govindarajan, S., and Paul, S., Appl. Surf. Sci. 506, 144686 (2020).
[28] Neamen, D.A., in Microelectron. Circuit Anal. Des., 4th, illustr ed. (McGraw-Hill, 2010), pp. 126–204.
[29] Ortiz-Conde, A., García-Sánchez, F.J., Muci, J., Terán Barrios, A., Liou, J. J., and Ho, C.-S., Microelectron. Reliab. 53, 90 (2013).